Microstructure and Materials Characterization of Sol-Gel Synthesized ZrO$_2$ Systems

Sungsoo Park[1] and Godlisten N Shao[2*]

[1]*Department of Fusion Chemical Engineering, Hanyang University, 1271 Sa 3-dong, Sangnok-gu, Ansan-si, Gyeonggi-do 426-791, Republic of Korea*
[2]*Department of Chemistry, Mkwawa College, University of Dar es Salaam, P. O. Box 2513, Iringa, Tanzania*
[*]*Corresponding author e-mail address: shaogod@gmail.com*

Abstract

The roles of pH and thermal treatment on the microstructures of sol-gel synthesized mesoporous ZrO$_2$ systems have been investigated. In order to control the crystal structures and particle sizes of the final products, the pH values of the reaction mixtures were controlled between 5 and 12 followed by calcination at temperatures ranging from 450 to 1000 °C. The microstructures of the zirconia systems were then examined by XRD, TEM, TGA, UV-visible DRS and nitrogen physisorption study analyses. It was found that pH values and calcination temperatures have significant influence on the crystallization temperature, phase transformation and particle size of the ZrO$_2$ systems. Pure tetragonal and monoclinic ZrO$_2$ crystals or a mixture of tetragonal and monoclinic ZrO$_2$ crystals with controlled particle size could readily be yielded by maintaining the pH values and the calcination temperatures. This study therefore elucidates a facile approach to yielding sol-gel synthesized metal oxide nanoparticles with controlled phase and particle size.

Keywords: Microstructure; Zirconia systems; Sol-gel process; Phase transformation.

Introduction

ZrO$_2$ is one of the most important ceramic materials that exhibit excellent mechanical, thermal, corrosion resistance and dielectric properties (Becker et al. 2008, Shao et al. 2014, Cao et al. 2015). Zirconia has been widely used in engineering ceramics (Becker et al. 2008), pressurized water reactors (Simeone et al. 2000), gas and humidity sensor technology (Cosentino et al. 2003, Cao et al. 2015), fuel cell technology (Becker et al. 2008, Cimenti and Hill 2009), catalyst support (Shao et al. 2014), electro-optical (Becker et al. 2008), medicines (Al-Amleh et al. 2010, Cao et al. 2015) and magnetics (Cao et al. 2015). It can exist as monoclinic (m-ZrO$_2$), tetragonal (t-ZrO$_2$) and cubic (c-ZrO$_2$) phases (Berry et al. 1999, Simeone et al. 2000, Cosentino et al. 2003, Becker et al. 2008, Cimenti and Hill 2009, Al-Amleh et al. 2010, Mamivand et al. 2013, Shao et al. 2014, Cao et

al. 2015). Tetragonal and cubic zirconia crystals are unstable at room temperature. In bulk materials, ZrO$_2$ exists as a monoclinic phase which is stable at room temperature up to ~1170 °C. The monoclinic phase transforms to tetragonal upon calcination at temperatures higher than ~1170 °C whereas the cubic structures can be obtained at temperatures higher than 2300 °C (Patil and Subbarao 1970, Srinivasan et al. 1991, Simeone et al. 2000, Cosentino et al. 2003, Simeone et al. 2006, Spijksma et al. 2006, Al-Amleh et al. 2010, Davar et al. 2013, Gómez et al. 2013, Shao et al. 2014, Cao et al. 2015).

Various studies have shown that phase structure, particle size and morphology of the final product can influence the applications of the ZrO$_2$ (Stichert and Schüth 1998, Rhodes and Bell 2005, Li et al. 2008). Apparently, various preparation approaches that facilitate the formation of zirconia systems with

190

desirable properties for different applications have been delineated. These include sol-gel, hydrothermal, co-precipitation, solvothermal, ultrasonic spray pyrolysis, emulsion precipitation, thermal decomposition and microwave/sonication-assisted methods (Patil and Subbarao 1970, Srinivasan et al. 1991, Simeone et al. 2000, Cosentino et al. 2003, Simeone et al. 2006, Spijksma et al. 2006, Zhao et al. 2006, Davar et al. 2013, Gómez et al. 2013, Shao et al. 2014, Cao et al. 2015, Manoharan et al. 2015). However, the sol-gel process has been enormously used as it allows the preparation of products with better homogeneity and distribution. Commonly, the formation of zirconia systems with stable phases is a challenge to many researchers (Patil and Subbarao 1970, Berry et al. 1999, Ding et al. 2015, Manoharan et al. 2015, Ding et al. 2017). Needless to say, the performance of the final products is enhanced if the resulting material demonstrates stable phase structure and microstructures.

The incorporation of stabilizing dopants such as Y^{3+}, Mg^{2+}, and Ca^{2+} or crystallite size reduction strategies are some of the approaches that have been applied to harness phase stability of ZrO_2 crystals at room temperature (Patil and Subbarao 1970, Ding et al. 2015, Manoharan et al. 2015, Ding et al. 2017). However, incorporation of impurities can hinder some of the other applications that require pure ZrO_2 nanomaterials such as the preparation of efficient optical films. Berry et al. (1999) reported the influence of pH on zirconia formed from zirconium (IV) acetate solution by hydrothermal approach. It was unveiled that zirconia formed from a solution of high pH contained a greater quantity of the tetragonal and cubic zirconia. Notably, this hydrothermal technique is tedious and requires expensive equipment and complicated routes to obtain final products. From this view point, the design facile and cost-effective preparation methods to enhance phase stability and controlling morphologies of pure ZrO_2

nanostructures are indisputably in great demand.

Srinivasan et al. (1991) reported a useful technique to identify tetragonal and cubic structures of ZrO_2 synthesized through different conditions. Zhao et al. (2006) reported the synthesis of shape-controlled colloidal ZrO_2 nanocrystals through hydrothermal techniques using a mixture of toluene solution, zirconia precursors and various acids. Through their preparation method, different crystal structures and phase were formed at different temperatures and monomer concentrations. Yan et al. (2009) synthesized ZrO_2-TiO_2 with monodispersed microspheres using titanium and zirconium alkoxides. Cao et al. (2015) reported the fabrication of porous ZrO_2 nanostructures with controlled crystalline phases and structures via a cost-effective hydrothermal approach as well. These versatile reports demonstrate that morphology, phase, particle size and shape of materials are strongly dependent on the precursors, preparation method and treatment of the final product. However, these preparation methods utilize complex procedures and precursors as well as special and expensive equipment which hinders large-scale production and commercialization of the final products. Cao et al. (2015) further observed that the resulting ZrO_2 system displays poor crystallinity, irregular particles with broad size distribution, and low surface area. Thus, the design of new approaches to fabricate zirconia nanostructures with improved physico-chemical properties such as small particle sizes, high crystallinity, high surface area etc., can enhance large-scale production and commercialization of zirconia systems.

Consequently, our research group has carried out various studies (Hilonga et al. 2010a, Shao et al. 2012a, Shao et al. 2012b, Kim et al. 2013, Shao et al. 2013a, Shao et al. 2014) toward production of metal oxide systems with favorable properties such as high crystallinity and homogeneous product with an

even distribution of primary particles for myriad of applications such as photocatalysis, gas sensors and energy conversion. The utilization of non-alkoxide precursors and sol-gel process has been extremely vital in forming products with promising physico-chemical properties. It is observed that the formation of metal oxide sols from precursors is the one that facilitates a controllable and rapid reaction at ambient conditions (Leoni et al. 2001, Salahinejad et al. 2012a, Salahinejad et al. 2012b, Salahinejad et al. 2013, Verma et al. 2013, Shao et al. 2014).

In this study, a cost-effective, controllable, reproducible and versatile sol-gel process to produce mesoporous ZrO_2 nanostructures with controlled morphology and crystalline structures using zirconyl nitrate hydrate as a zirconia precursor has been introduced. Generally, zirconyl nitrate is water soluble Lewis acid which can be employed in the synthesis of various ZrO_2 nanostructures of different morphologies and crystal structures. Being a very strong acid, the consumption of inorganic acids such as H_2SO_4, HNO_3 or HCl during the synthesis process can essentially be precluded. Therefore, designing a systematic preparation technique that yields ZrO_2 systems with stable crystal structures and size using $ZrO(NO_3)_2$ (a rarely reported precursor) would be economical and can substantially enhance large-scale production ZrO_2 systems. In order to attain products with tuned morphology and particle sizes, the as-synthesized samples were obtained at different pH values ranging from 5 to 12 and then calcined at different temperatures.

Materials and Methods

Zirconyl nitrate (99%) and cetyltrimethylammonium bromide (CTAB, 99%) were procured from Sigma-Aldrich. Sodium hydroxide beads (99%) were purchased from DS Chemicals Ltd. All chemical reagents were used as received from commercial sources without further purification. Zirconia systems were synthesized via a modified sol-gel method. In a typical experiment, 100 mL of distilled water and 0.5 g CTAB were added into four different beakers and the solutions were stirred for 30 min. 0.05 mol of zirconyl nitrate hydrate was then added in each beaker to obtain solution A1, A2, A3 and A4, respectively. The solutions were stirred at room temperature for further 30 min and the pH of the solutions was ~1. The pH of the solutions was then adjusted using 0.5 M sodium hydroxide solution from 1 to 5, 7, 9 and 12 in solutions A1, A2, A3 and A4, respectively. The reaction mixtures were held at room temperature for 6 h to enhance aging under constant stirring. After aging the solutions were centrifuged to remove CTAB and Na^+. The samples were then washed with water and ethanol and the recovered gels were oven dried at 70 °C for 12 h. The dried samples were ground thoroughly and were dubbed Z5-00, Z7-00, Z9-00 and Z12-00 for the as-synthesized samples obtained at pH 5, 7, 9 and 12, respectively. The as-prepared samples were calcined in a box furnace at 450, 650, 850 and 1000 °C for 2 h. The calcined samples were dubbed ZX-Y samples; where X is the pH and Y is the calcination temperature. For example, the sample obtained at pH 12 and calcined at 450 °C was labeled Z12-450. The preparation process is summarized in Scheme 1.

```
┌─────────────────────────────────────┐
│        1) Conditioning agent         │
│  Cetyl trimethyl ammonium bromide    │
│             (CTAB)                   │
│            2) Solvent                │
└─────────────────────────────────────┘
┌─────────────────────────────────────┐
│           3) Precursor               │
│    0.05 M ZrO(NO₃)₂.xH₂O             │
└─────────────────────────────────────┘
┌─────────────────────────────────────┐
│           4) Titration               │
│    pH 5, 7, 9.12 by 0.5 M NaOH       │
└─────────────────────────────────────┘
┌─────────────────────────────────────┐
│            5) Aging                  │
│         For 4 h at 80 °C             │
└─────────────────────────────────────┘
┌─────────────────────────────────────┐
│         6) Centrifugation            │
│   8000 rpm at 10 min by Et-OH 2      │
│        times, H₂O 2 times            │
└─────────────────────────────────────┘
┌─────────────────────────────────────┐
│          7) Calcination              │
│          At 450 -1000 °C             │
└─────────────────────────────────────┘
┌─────────────────────────────────────┐
│              ZrO₂                    │
│     (Amorphous, crystalline)         │
└─────────────────────────────────────┘
```
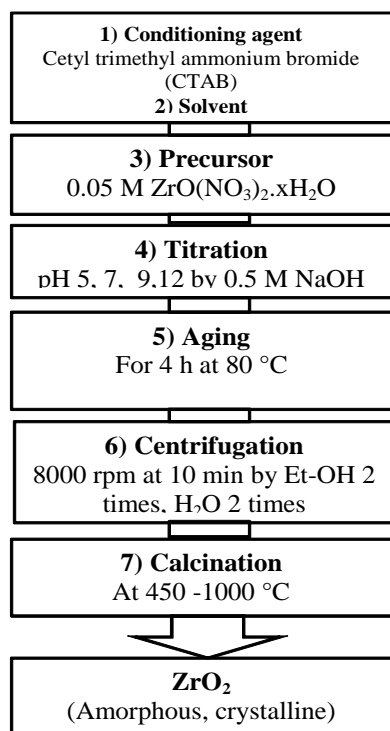
Scheme 1: Schematic preparation approach for ZrO_2 nanoparticles.

The crystal structures of the samples were studies by powder XRD analysis. An X-ray diffractomer (XRD, Rigaku, Japan) was used to examine the characteristics of diffractograms of the samples using Cu Kα. The accelerating voltage and applied current were 40 kV and 100 mA, respectively. The crystallite size of the ZrO_2 systems were then estimated by the Scherer-Debye equation, $D = K\lambda/\beta Cos\Theta$ where constant, $K = 0.9$; wavelength of the emitted light, $\lambda = 0.15406$ nm; β is the full width at half maximum (FWHM) of the diffraction peak in radians and θ is the Bragg's angle (Tanemura et al. 2003). The characteristic peaks of monoclinic [-111] peak at $2\Theta = 28°$ and tetragonal [101] at $2\Theta = 30°$ were chosen to estimate the particle size of the systems. Field emission scanning electron microscopy (JEOL, JSM-6701F, Japan) was used to study the morphology of the ZrO_2

powders at a working distance of 8 mm with an accelerating voltage and current of 40 kV and 150 mA, respectively. High-resolution transmission electron microscopy (HRTEM, Jeol JEM 2100F, Korea) was used to study the particle size and distribution.

The thermal stability/ properties of the as-synthesized ZrO_2 samples was monitored using a differential thermal-thermogravimetric analyzer (NETZSCH STA 409PC, Germany) in nitrogen gas atmosphere with temperature ranging from room temperature to 850 °C. This process was monitored under nitrogen gas atmosphere at a flow rate of 10 ml/min and a heating rate of 10 °C/ min. The diffuse reflectance spectra (DRS) of the samples were recorded by a UV-vis spectrophotometer (Shimadzu, UV-2600) from 200 to 900 nm using $BaSO_4$ as a reference. The Brunauer-Emmett-Teller (BET) surface area and the porosity of the samples were studied by a nitrogen adsorption-desorption instrument (Tristar, Germany) at 77 K. All the samples measured were degassed at 200 °C for 2 h prior to actual analysis. Pore size distribution (PSD) and specific desorption pore volumes were obtained using the Barrett-Joyner-Halenda (BJH) method and desorption branches were used to determine the PSD. The optical properties of the ZrO_2 systems were investigated by the UV–visible diffusive reflectance spectrometry (UV–vis DRS). The reflectance spectra were calculated by Kubelka-Munk theory (KM,α) and then Tauc's plot was constructed from (KM. *hv*) ½ against hυ to obtain the band gap of the samples (Goharshadi and Hadadian 2012, Shao et al. 2014).

Results and Discussion
Thermal properties
Figure 1 shows that the initial mass loss at ~100 °C was attributed to the partial evaporation of water present on the surface of the nanopowders. The thermograms reveal another weight loss at ~200 °C which is ascribed to the removal of the physically

adsorbed water (Benjume 2012, Shao et al. 2014). The weight loss observed at temperatures ranging from 200-400 °C is associated with the decomposition of the surfactant and subsequent crystallization of zirconia due to the dehydration of zirconium hydroxides to form Zr-O-Zr networks (Yuan et al. 2009, Shao et al. 2014). The thermograms can further reveal that the thermal stability of the synthesized ZrO_2 systems increased as the pH values were increased. Generally, the weight loss registered in the sample obtained at pH 5 was ~43% whilst a weight loss of < 20% was observed in the sample obtained at pH 12. It is noteworthy that the final zirconia nanopowders obtained through this preparation method at different pH values were between 60 and 80 wt. % which are greater than that obtained using sonochemical method (Manoharan et al. 2015). These results therefore signify that heating of the systems at temperatures > 400 °C is sufficient to remove the surfactant and enhance crystallization.
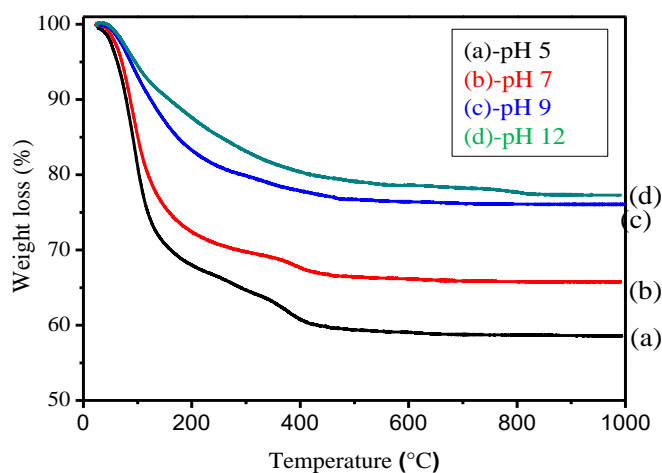
Figure 1: TGA profiles of the as-synthesized ZrO_2 nanoparticles obtained at different pH values; (a) pH 5, (b) pH 7, (c) pH 9 and (d) pH 12.

Crystal structure

The XRD diffractograms for the ZrO_2 samples obtained at pH values of 5, 7, 9 and 12 and calcined at temperatures of 450, 650, 850 and 1000 °C are depicted in Figures 2-5. Initially, the XRD diffractograms of all of the as-synthesized samples (not presented) showed the presence of an amorphous structure regardless of the pH value used to synthesize the powders. The calcined samples demonstrated the formation of different crystal structures depending on the pH values and calcination temperature. Figure 2 shows the XRD diffractograms of the samples obtained at different pH values and then calcined at 450 °C. It is evident that the samples obtained at lower pH values of 5, 7 and 9 demonstrated the presence of crystalline zirconia while the sample obtained at high pH value of 12 was still amorphous. These samples showed the emergence of tetragonal ZrO_2 crystals at $2\theta =$ 30°, 35°, 50°, 60°, 63° and 74° (Pérez et al. 2008, Gómez et al. 2013, Shao et al. 2014).

The XRD diffractograms of samples synthesized at different pH values and calcined at 650 °C are shown in Figure 3. In this case, the samples obtained at higher pH values of 9 and 12 revealed the presence of t-

ZrO_2 peaks whereas a mixture of monoclinic ZrO_2 crystals (m-ZrO_2) and t-ZrO_2 can be observed in samples synthesized at lower pH values of 5 and 7. The peaks depicting the existence of m-ZrO_2 can be seen at $2\theta = 28°$, 31° and 34° (Srinivasan et al. 1991, Yuan et al. 2009, Shao et al. 2014). Another striking feature can be observed in samples calcined at 850 °C (Figure 4) from which it can be seen that samples synthesized at pH values of 5, 7 and 9 showed the presence of only m-ZrO_2 while a mixture of m-ZrO_2 and t-ZrO_2 is observed in the Z12-850 sample. Interestingly, Figure 5 indicates that all samples calcined at 1000 °C demonstrated the existence of t-ZrO_2. Hence, it is very clear that the formation of different crystal structures was dependent on the synthetic conditions and calcination temperature with high calcination temperatures resulting in formation of more crystalline phases. This shows that formation of different ZrO_2 crystals can be accomplished through sol-gel approach by adjusting the pH values and calcination temperatures.
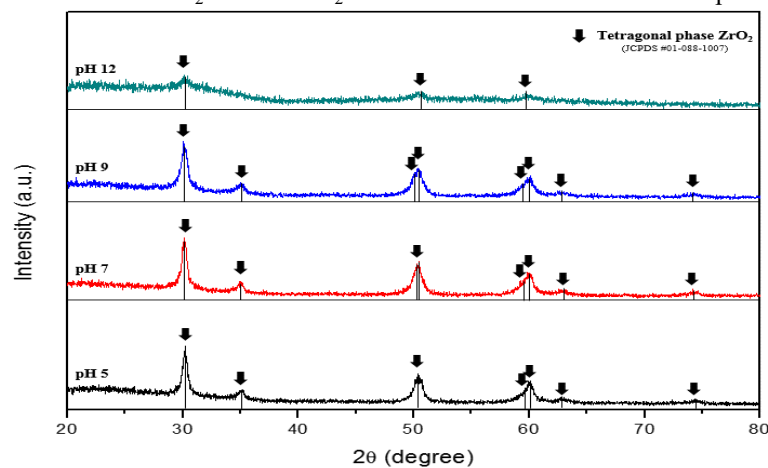
Figure 2: XRD patterns of ZrO_2 nanoparticles obtained at different pH values and calcined at 450 °C.
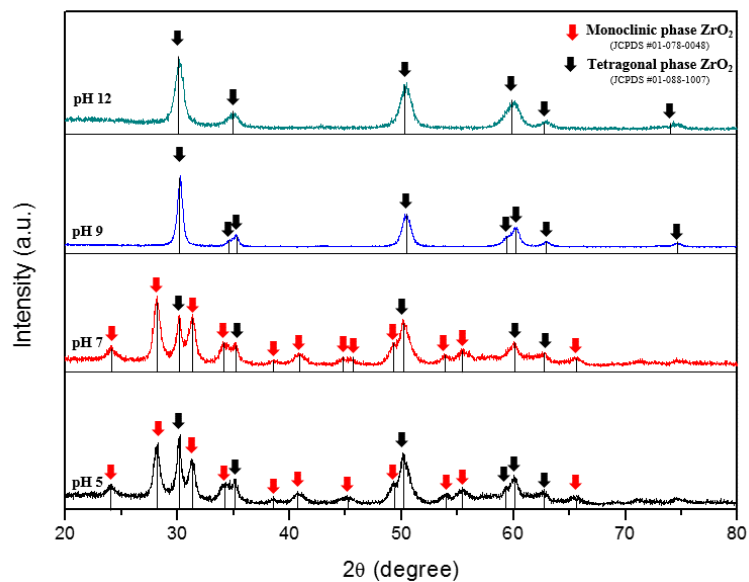
Figure 3: XRD patterns of ZrO_2 samples synthesized at different pH values and calcined at 650 °C.
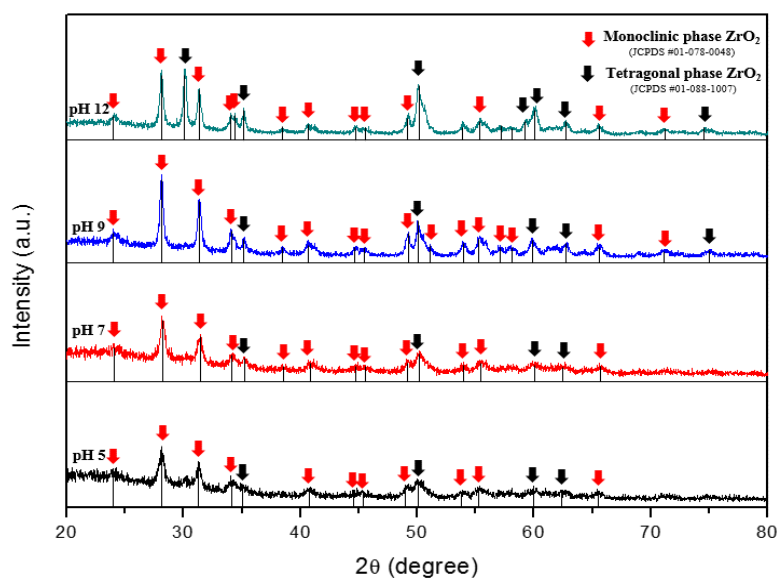
Figure 4: XRD patterns of ZrO_2 samples synthesized at different pH values and calcined at 850 °C.

196
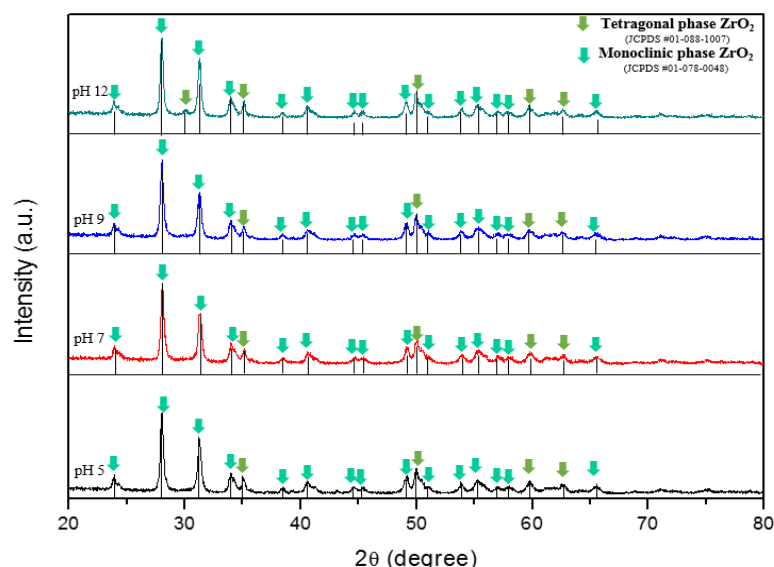
Figure 5: XRD patterns of ZrO_2 samples synthesized at different pH values and calcined at 1000 °C.

The crystallite size of the samples was estimated using the Scherer-Debye equation and the results are shown in Table 1. It can be observed that samples calcined above 650 °C had nearly uniform crystallite sizes (10-12 nm) regardless of the pH value used to synthesize the ZrO_2 systems. Only samples Z9-850 and Z12-850 displayed larger average particle sizes of 17 and 22 nm, respectively. Generally, the pH of the solution was a critical factor in controlling the crystal structure and average particle size of the ZrO_2 systems. A close analysis of the XRD results indicates that (i) change in pH values has no significant effect on the average particle size of the samples calcined up to 650 °C, and (ii) calcination of the zirconia samples promotes phase transformation from amorphous $\rightarrow$ tetragonal $\rightarrow$ monoclinic + tetragonal $\rightarrow$ monoclinic ZrO_2 crystals.

Table 1: Average grain size of different zirconia samples obtained at different conditions

Sample name /Calcination Temperature (°C)	Crystallite size (nm)			
	450 °C	650 °C	850 °C	1000 °C
Z5	11.5 (t)	11.6 (m + t)	11.8 (m)	18.2 (m)
Z7	11.8 (t)	11.1 (m + t)	12.7 (m)	20.6 (m)
Z9	10.1 (t)	11.0 (t)	17.1 (m + t)	24.1 (m)
Z12	-	10.9 (t)	21.7 (m + t)	29.4 (m)

m= monoclinic; t = tetragonal

Nitrogen gas adsorption-desorption properties

The N_2 gas adsorption-desorption isotherms of the samples obtained at different conditions are presented in Figure 6 whereas the BET surface areas and porosities of the samples are displayed in Table 2. Generally, the as-synthesized samples possessed high

surface areas (140–360 m^2/g) with that of Z7-00 (369 m^2/g) being the highest. It can be seen that the surface areas decreased (32–45 m^2/g) upon calcination as a result of crystallization (Yuan et al. 2009, Shao et al. 2012a, Shao et al. 2014). However, the pore sizes of the calcined systems were relatively larger than those of raw samples indicating that the removal of the surfactant through calcination generates products with large pore sizes.

Still from Figure 6, it can be observed that different isotherms were displayed depending on the pH value and calcination temperature. Figure 6a indicates that the isotherms of the as-synthesized were more or less of type IV portraying the formation of mesoporous nanostructures. The hysteresis of these samples demonstrate that the nitrogen gas uptake was centered at relative pressures $0.4 < P/P_o < 0.85$. On the other hand, the samples calcined at 450 and 650 °C (Figures 6b and c) showed the presence of Type IV which signifies the existence of mesoporous structures associated with capillary condensation of the nitrogen gas adsorbent. The nitrogen gas uptake in these samples occurred at relative pressures $0.45 < P/P_o < 0.95$. The as-synthesized samples and samples calcined at 450 °C possessed hysteresis loops that are very close to Type H2 according to the IUPAC classification system. Type H2 hysteresis loop depicts that the samples consisted of aggregates with neck-bottle pores (Shao et al. 2014, Cao et al. 2015, Shao et al. 2015a, Shao et al. 2013a, Shao et al. 2015b, Sheikh et al. 2015) . The Z9-650, Z12-650 and Z9-850 samples exhibited a Type H1 hysteresis loop that demonstrates the presence of compact agglomerate of approximately cylindrical-like pores. Meanwhile, Figure 6d reveals that the Z12-850 sample possessed Type H4 hysteresis loop indicating the presence of narrow, slit-like pores (Hilonga et al. 2010b, Shao et al. 2012a, Shao et al. 2013b).

Table 2: BET Surface area, pore volume and pore diameter distribution of the as-synthesized and calcined samples of ZrO_2 samples by different pH

Sample name	Surface area (m^2/g)	Pore volume (cm^3/g)	Pore size (nm)
Z5-00	285	0.13	2.5
Z7-00	369	0.24	2.8
Z9-00	264	0.17	2.7
Z12-00	284	0.25	3.0
Z5-450	90	0.07	2.9
Z7-450	95	0.08	2.9
Z9-450	196	0.20	3.2
Z12-450	139	0.13	3.2
Z5-650	30	0.07	5.5
Z7-650	44	0.10	6.4
Z9-650	44	0.12	7.8
Z12-650	30	0.12	13.2
Z5-850	8	0.03	4.5
Z7-850	8	0.03	4.3
Z9-850	12	0.09	24.4
Z12-850	9	0.01	5.5
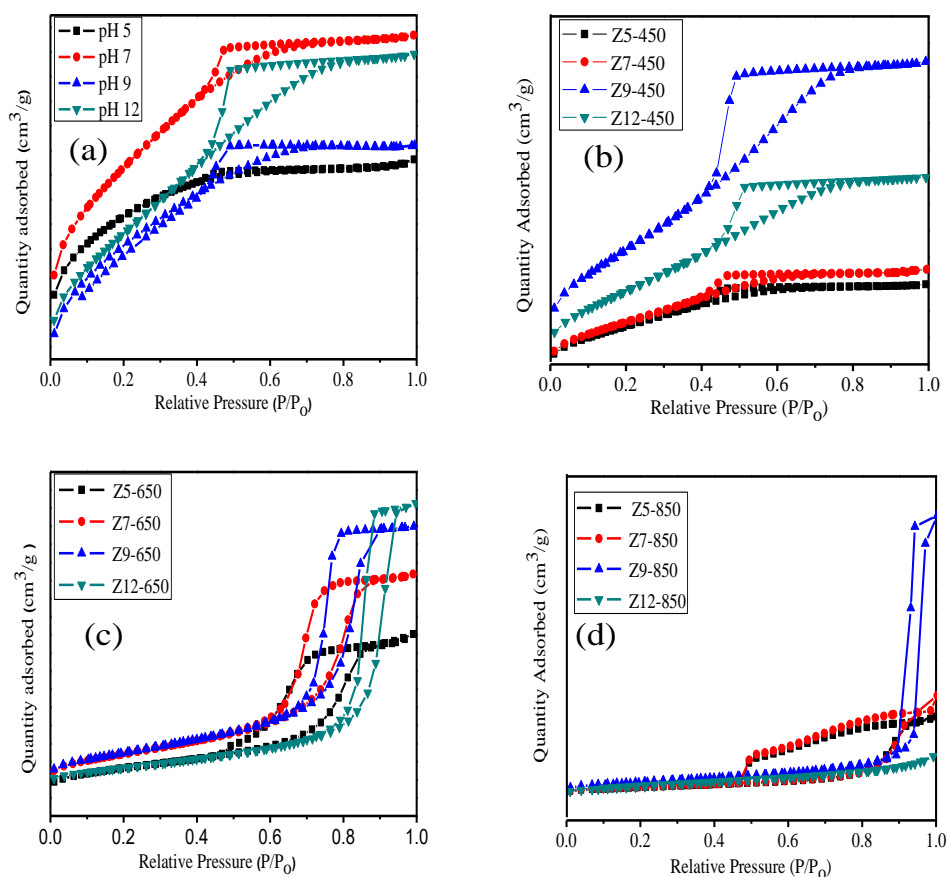
Figure 6: Nitrogen gas adsorption-desorption isotherms of ZrO_2 samples obtained at different pH values; (a) as-synthesize samples, (b) sample calcined at 450 °C, (c) 650 °C, and (d) 850 °C.

Figure 7 presents the pore size distribution (PSD) of the ZrO_2 systems obtained at different conditions. It can be seen that the PSD of the as-synthesized samples and those calcined up to 650 °C possessed approximately similar patterns. The PSD of the as-synthesized samples (Figure 7a) ranged from 2 to 4.3 nm while those of the calcined samples are between 2 and 18 nm (Figures 7b and c). It is obvious that the pore sizes increased as the calcination temperature was increased due to the removal of the surfactant and crystallization of the samples (Shao et al. 2014). Figure 7d reveals the samples calcined at 850 °C had both mesoporous and macroporous structure.
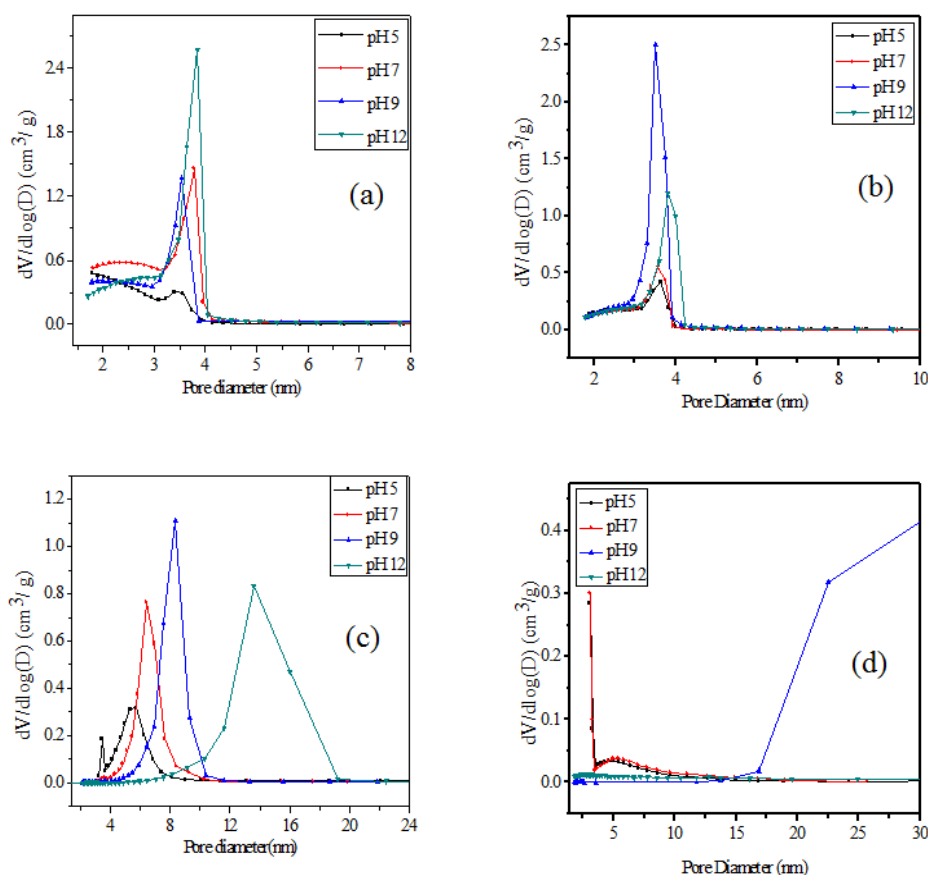
Figure 7: Pore size distribution of the ZrO_2 nanoparticles obtained at different pH values; (a) as-synthesized samples (b) 450 °C (c) 650 °C and (d) 850 °C.

Morphology of ZrO₂ systems

The SEM images showing the effect of pH and calcination temperature in the ZrO_2 samples are displayed in Figures 8 to 10. Generally, these samples displayed different morphologies depending on the pH and calcination temperature. Figure 8 shows that the samples synthesized at pH values of 5, 7, 9 and 12 and calcined at 450 °C comprised of mainly irregular and compact spherical aggregates. Nonetheless, Figures 9 and 10 demonstrate that through calcination of the as-prepared samples at 650 and 850 °C, materials

with less aggregated primary particles were yielded. It is noteworthy that the samples calcined at 850 °C generated ordered primary particles indeed. This indicates that pH value and calcination temperature are significant parameters to control the sizes and distribution of the particles in ZrO_2 based nanostructures. The zirconia systems were composed of aggregates with average diameter less than 20 nm as depicted in Figures 8 to 10. These results are therefore in good agreement with the XRD results (Table 1).

200
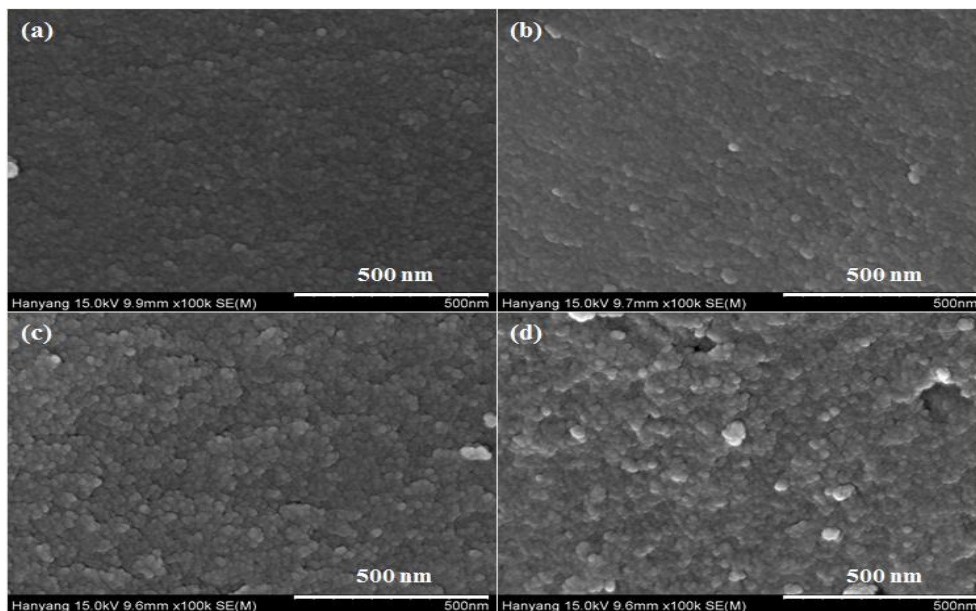
Figure 8: SEM images of the ZrO_2 samples synthesized at different pH values and calcined 450 °C (a) pH 5, (b) pH 7, (c) pH 9 and (d) pH 12.
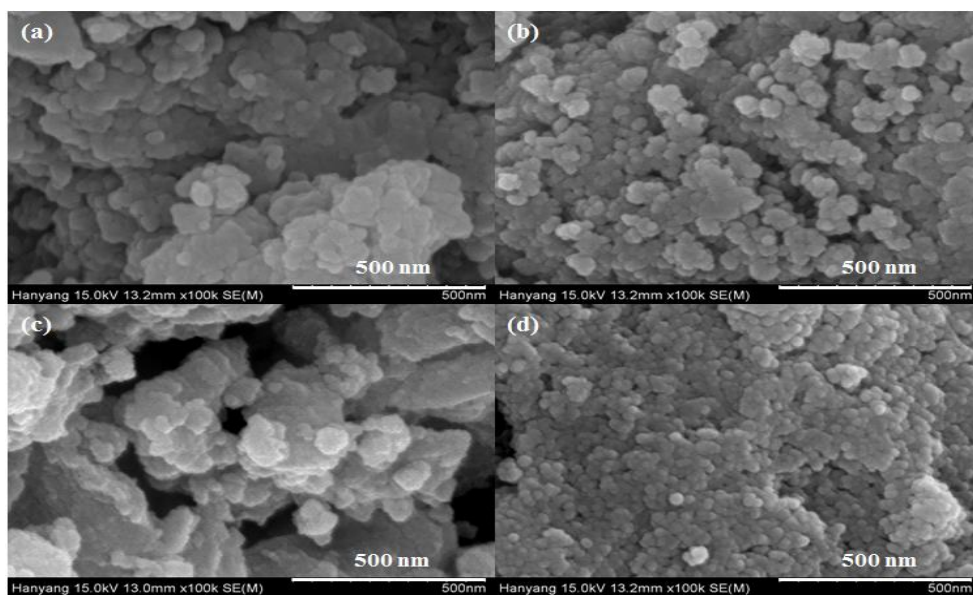
Figure 9: SEM images of the ZrO_2 samples synthesized at different pH values and calcined 650 °C (a) pH 5, (b) pH 7, (c) pH 9 and (d) pH 12.
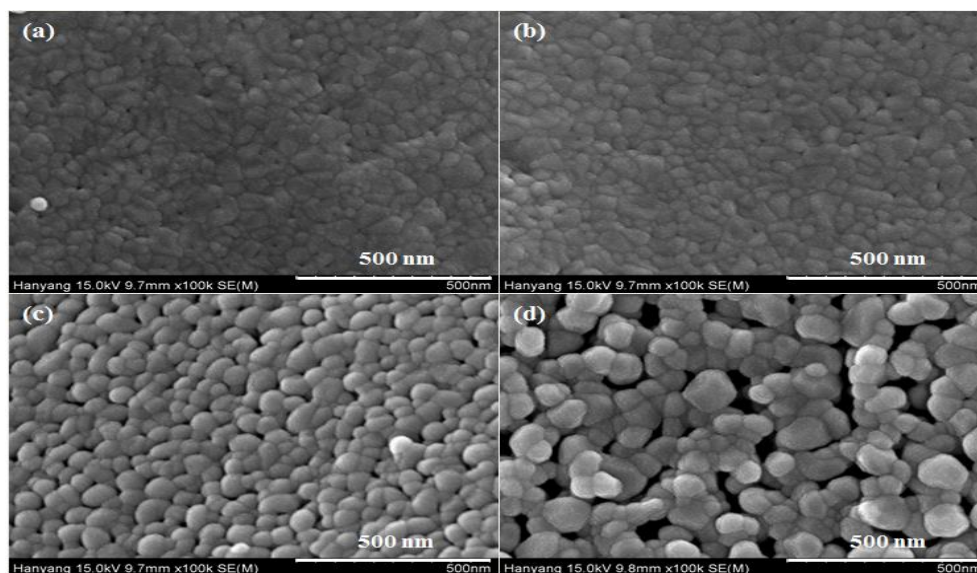
Figure 10: SEM images of the ZrO_2 samples synthesized at different pH values and calcined 850 °C (a) pH 5, (b) pH 7, (c) pH 9 and (d) pH 12.

Furthermore, SEM results of the present study are congruent with those available in the previously reported studies (Hanaor et al. 2012, Shao et al. 2014). Shao et al. (2014) investigated the influence of ZrO_2 content in the microstructures of ZrO_2-TiO_2 composites. It was observed that the morphologies of the obtained samples were dependent on the ZrO_2 content and the calcination temperatures. Generally, the samples obtained at 600 °C to 800 °C generated less-aggregated, ordered and large particles as a result of grain growth. It was previously reported (Bhattacharyya et al. 2009, Parkinson 2013) that during calcination grain growth occurs through cluster diffusion-coalescence or by Ostwald ripening. It can further be deduced that calcination facilitated the formation of more porous structures. These results are congruent with the BET and nitrogen gas physisorption studies presented in Table 2.

The High Resolution TEM (HR-TEM) images of the zirconia systems obtained at 650 °C at different pH values are compiled in Figure 11. These images reveal the presence of crystalline structures of primary particles as depicted by the XRD analysis. It can be seen that the systems consisted of small particles less than 20 nm. Figure 11 indicates that the Z5-650 and Z7-650 samples showed lattice spacing of 0.293 nm and 0.322 nm assignable to the tetragonal and monoclinic ZrO_2 crystals, respectively. This signifies that a mixture of the tetragonal and monoclinic ZrO_2 crystals can be attained through phase transformation upon calcination at 650 °C. On the other hand, the Z9-650 and Z12-650 samples showed lattice spacing for only tetragonal ZrO_2 crystals. Consequently, the grain size observed from TEM analysis is very close to that was estimated by the Scherer equation (Table 1). Another interesting observation is that the rates of aggregation of the synthesized zirconia systems differ depending on the pH values as well. It can be seen that the particles obtained at pH 5 were more aggregated than grains yielded at pH 12. These results are more or less consistent with the SEM analysis (Figures 8-10).
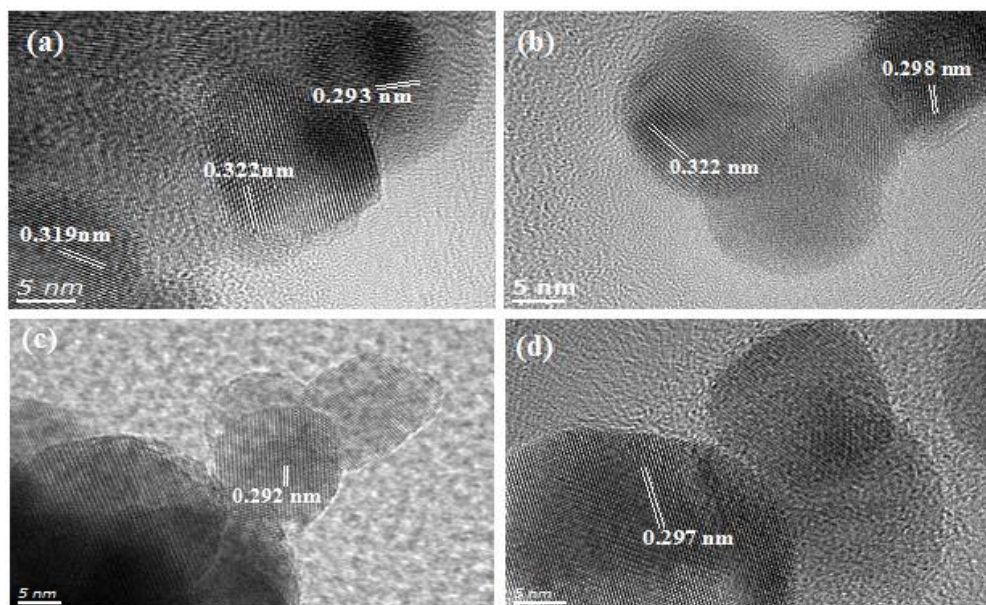
Figure 11: HR-TEM images of the ZrO_2 samples synthesized at different pH values and calcined at 650 °C; (a) Z5-650 (b) Z7-650 (c) Z9-650 (d) Z12-650.

Goharshadi and Hadadian (2012) reported the preparation of ZrO_2 systems via the hydrolysis of zirconyl nitrate in aqueous–alcohol solution using microwave irradiation. It was found out that the TEM analysis of the samples calcined at 500 °C registered an average particle size of about 27 nm. This observation indicates that the ZrO_2 samples obtained by the sol-gel method in the present study exhibited smaller particle sizes than those reported by Goharshadi and Hadadian (2012). Even though both studies utilized the same precursor, but different preparation methods were employed. Hence, the preparation technique can facilitate the formation of final products with different physico-chemical properties regardless on the nature of the starting materials.

Optical properties

Figure 12 shows the DRS spectra of the ZrO_2 systems obtained at different conditions. All reflectance spectra of the samples revealed an absorption edge less than 400 nm which is a result of ligand-to-metal charge transfer in ideal ZrO_2 systems between the interaction of the O^{2-} ligand and the Zr^{4+} ion. The spectra registered absorption in the near UV and visible region that is most likely a result of transitions involving extrinsic states such as surface trap states or structural defect states (Manoharan et al. 2015).

The band gaps (E_g) of the samples were obtained from the energy intercept by extrapolations of the straight regions of the absorption coefficient $(\alpha hv)^2$ versus photon energy (hv) for a direct allowed transition as presented in Figure 13. It can be seen that the band gap of the calcined samples (Figure 13b) were smaller than those of the as-synthesized samples (Figure 12a).The band gaps of the calcined samples seem to increase with increasing pH values. It can also be noticed that the band gaps decreased with increasing crystallite sizes demonstrating the existence of quantum confinement phenomena. Moreover,

the bad gap energies obtained in the present study were smaller than those reported in the previous studies (Goharshadi and Hadadian 2012, Manoharan et al. 2015, Patel et al. 2016). This reveals that the proposed cost-effective preparation method and precursor can be used for the formation of ZrO_2 systems with promising physico-chemical properties and can boost large-scale production and commercialization of zirconia based systems.
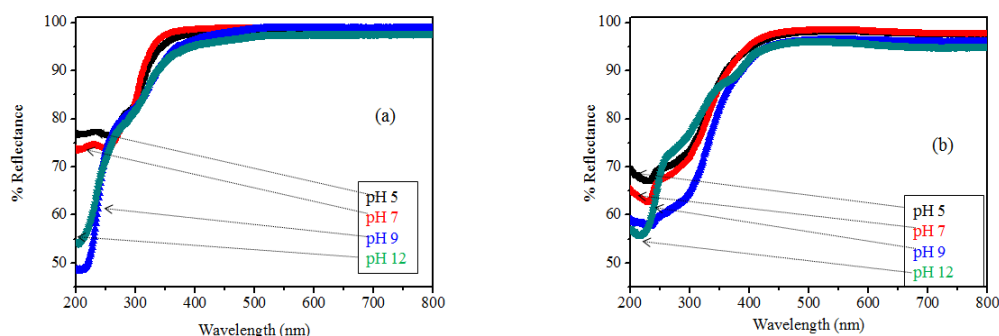
Figure 12: UV-visible diffuse reflectance spectra of the as synthesized amorphous (a) and crystalline (b) ZrO_2 samples calcined at 650 °C.
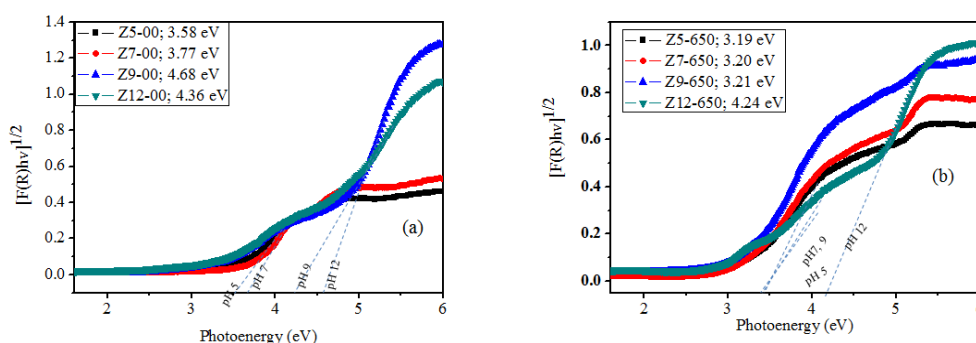
Figure 13: Band gap energy of ZrO_2 samples estimated using Kubelka-Munk equation (a) amorphous and (b) calcined at 650 °C from Tauc's plot.

The roles of pH and calcination temperatures in influencing the physico-chemical properties of metal oxides have been widely investigated (Berry et al. 1999, Mamivand et al. 2013). Berry et al. (1999) noticed that the pH of the reaction mixture can influence the crystal structures of the ZrO_2 systems obtained using zirconium (IV) acetate precursor. The report indicated that ZrO_2 materials formed at high pH contain large quantity of tetragonal phase due to the presence of –OH groups that are presumed to suppress the tetragonal to monoclinic phase transition (T $\rightarrow$ M) (Matsui et al. 1995, Berry et al. 1999). Accordingly, the present study demonstrated that the T $\rightarrow$ M can occur when the powders obtained at different pH values are calcined at different temperatures. XRD and SEM analyses indicated that the particle sizes of the samples calcined at different temperatures were more or less same. This signifies that phase transformation in metal oxides can be influenced by various factors such as the calcination temperature, nature of

the starting materials, incorporation of dopants/foreign atoms, synthetic method, particle size and pH of the reaction mixture (Berry et al. 1999, Becker et al. 2008, Shao et al. 2014, Manoharan et al. 2015). Further reports have also indicated that phase stabilization and phase change in zirconia particles are largely dependent of the critical size i.e., the critical size for the formation of tetragonal phase is 10 nm while the tetragonal and monoclinic phases co-exist between 11 and 30 nm (Becker et al. 2008).

The present study has demonstrated that the formation of ZrO_2 nanoparticles from $Zr(ONO_3)_2$ precursor involves the formation of $Zr(OH)_4$ gel which can eventually be dried to form amorphous powders of $Zr(OH)_4$. Calcination of the obtained amorphous gel leads to the formation of the Zr-O-Zr networks as a result of hydration and polymerization processes as was revealed by the TGA analysis. Thus, the formation of the Zr-O-Zr networks is associated with ZrO_2 phase formation and transformation as well (Berry et al. 1999, Mamivand et al. 2013, Shao et al. 2014). The results of the present study have shown that the T→M phase transformation was enhanced in the calcined samples synthesized at pH values of 5 and 7 while the T→M phase transformation was suppressed in the calcined samples synthesized at pH values of 9 and 12. It is evident that the presence of -OH groups stabilized the existence of the tetragonal crystal structure and delayed the T→M phase transformation (Matsui et al. 1995, Berry et al. 1999).

Conclusions

A systematic, convenient, reproducible, cost-effective and controllable preparation method to synthesize mesoporous zirconia nanoparticles was introduced. A modified sol-gel method was used to form zirconia systems with improved physico-chemical properties using zirconyl nitrate (rarely used precursors) at low reaction temperature and time. It was observed that the pH value of the reaction mixture, nature of the starting materials and the calcination temperature were factors that facilitated the formation of nanocrystals with specific crystal structures and morphology. The XRD and HRTEM analyses indicated that systems with either pure t-ZrO_2, m-ZrO_2 or a mixture of monoclinic and tetragonal ZrO_2 crystals can be achieved through varying the pH of the reaction mixture and calcination temperatures.

References

Al-Amleh B, Lyons K and Swain M 2010 Clinical trials in zirconia: a systematic review. *J. Oral Rehabil.* 37(8): 641-652.

Becker J, Hald P, Bremholm M, Pedersen JS, Chevallier J, Iversen SB and Iversen BB 2008 Critical size of crystalline ZrO_2 nanoparticles synthesized in near- and supercritical water and supercritical isopropyl alcohol. *ACS Nano.* 2(5): 1058-1068.

Berry FJ, Skinner SJ, Bell IM, Clark RJ and Ponton CB 1999 The influence of pH on zirconia formed from zirconium (IV) acetate solution: characterization by X-ray powder diffraction and Raman spectroscopy. *J. Solid State Chem.* 145(2): 394-400.

Bhattacharyya S, Höche T, Jinschek JR, Avramov I, Wurth R, Müller M and Rüssel C 2009 Direct evidence of Al-rich layers around nanosized $ZrTiO_4$ in glass: putting

the role of nucleation agents in perspective. *Cryst. Growth Des*. 10(1): 379-385.

Cao W, Kang J, Fan G, Yang L and Li F 2015 Fabrication of porous ZrO_2 nanostructures with controlled crystalline phases and structures via a facile and cost-effective hydrothermal approach: *Ind. Eng. Chem. Res*. 54(51): 12795-12804.

Cimenti M, and Hill JM 2009 Direct utilization of ethanol on ceria-based anodes for solid oxide fuel cells. *Asia-Pac. J. Chem. Eng*. 4(1): 45-54.

Cosentino IC, Muccillo ENS and Muccillo R 2003 Development of zirconia-titania porous ceramics for humidity sensors: *Sensor Actuat B: Chem*. 96(3): 677-683.

Davar F, Hassankhani A, and Loghman EMR 2013 Controllable synthesis of metastable tetragonal zirconia nanocrystals using citric acid assisted sol–gel method. *Ceram. Int*. 39(3): 2933-2941.

Ding Y, Long X, Peng S, Zhang D, Tan Z and Lu X 2017 Phase evolution and aqueous durability of $Zr_{1-x}-yCe_xNd_yO_{2-y/2}$ ceramics designed to immobilize actinides with multi-valences: *J. Nuc. Mater*. 487: 297-304.

Ding Y, Lu X, Tu H, Shu X, Dan H, Zhang S and Duan T 2015 Phase evolution and microstructure studies on Nd^{3+} and Ce^{4+} co-doped zircon ceramics. *J. Eur. Ceram. Soc*. 35(7): 2153-2161.

Goharshadi EK and Hadadian M 2012 Effect of calcination temperature on structural, vibrational, optical, and rheological properties of zirconia nanoparticles. *Ceram. Int*. 38(3): 1771-1777.

Gómez A, Villanueva R, Vie D, Murcia MS, Martínez E, Beltrán A, Sapiña F, Vicent M and Sánchez E 2013 Large scale synthesis of nanostructured zirconia-based compounds from freeze-dried precursors. *J. Solid State Chem*. 197: 120-127.

Hanaor DAH, Xu W, Ferry M and Sorrell CC 2012 Abnormal grain growth of rutile TiO_2 induced by $ZrSiO_4$. *J. Cryst. Growth*. 359: 83-91.

Hilonga A, Kim JK, Sarawade P, and Kim H 2010a Mesoporous titania–silica composite from sodium silicate and titanium oxychloride. Part I: grafting method. *J. Mater. Sci*. 45(5): 1255-1263.

Hilonga A, Kim JK, Sarawade PB and Kim HT 2010b Rapid synthesis of homogeneous titania-silica composite with high-BET surface area. *Powder Technol*. 199(3): 284-288.

Kim YN, Shao GN, Jeon SJ, Imran SM, Sarawade PB and Kim HT 2013 Sol–gel synthesis of sodium silicate and titanium oxychloride based TiO_2–SiO_2 aerogels and their photocatalytic property under UV irradiation. *Chem. Eng. J*. 231: 502-511.

Leoni M, Viviani M, Battilana G, Fiorello AM and Viticoli M 2001 Aqueous synthesis and sintering of zirconium titanate powders for microwave components. *J. Eur. Ceram. Soc*. 21(10–11): 1739-1741.

Li W, Huang H, Li H, Zhang W and Liu H 2008 Facile synthesis of pure monoclinic and tetragonal zirconia nanoparticles and their phase effects on the behavior of supported molybdena catalysts for methanol-selective oxidation. *Langmuir* 24(15): 8358-8366.

Garcia-Benjume ML, Espitia-Cabrera MI and Contreras-Garcia ME 2012 Enhanced photocatalytic activity of hierarchical macro-mesoporous anatase by ZrO_2 incorporation. *Int. J. Photoenergy* 2012 (Article ID 185159).

Mamivand M, Zaeem MA, El-Kadiri H and Chen LQ 2013 Phase field modeling of the tetragonal to monoclinic phase transformation in zirconia. *Acta Mater*. 61(14): 5223-5235.

Manoharan D, Loganathan A, Kurapati V and Nesamony VJ 2015 Unique sharp photoluminescence of size-controlled sonochemically synthesized zirconia nanoparticles. *Ultrason. Sonochem*. 23: 174-184.

Matsui K, Suzuki H, Ohgai M and Arashi H 1995 Raman spectroscopic studies on the formation mechanism of hydrous-zirconia fine particles. *J. Am. Ceram. Soc.* 78(1): 146-152.

Parkinson GS, Novotny Z, Argentero G, Schmid M, Pavelec J, Kosak R, Blaha P and Diebold U 2013 Carbon monoxide-induced adatom sintering in a Pd-Fe$_3$O$_4$ model catalyst. *Nat. mater.* 12: 724-728.

Patel US, Patel KH, Chauhan KV, Chawla AK and Rawal SK 2016 Investigation of various properties for zirconium oxide films synthesized by sputtering. *Proc. Technol.* 23 (Supplement C): 336-343.

Patil R, and Subbarao E 1970 Monoclinic–tetragonal phase transition in zirconia: mechanism, pretransformation and coexistence. *Acta Crystallogr. A* 26(5): 535-542.

Pérez-Hernández R, Mendoza-Anaya D, Fernández ME and Gómez-Cortés A 2008 Synthesis of mixed ZrO$_2$–TiO$_2$ oxides by sol–gel: microstructural characterization and infrared spectroscopy studies of NO$_x$. *J. Mol. Catal. A. Chem.* 281(1–2): 200-206.

Rhodes MD and Bell AT 2005 The effects of zirconia morphology on methanol synthesis from CO and H$_2$ over Cu/ZrO$_2$ catalysts: Part I. Steady-state studies. *J. Catal.* 233(1): 198-209.

Salahinejad E, Hadianfard M, Macdonald D, Karimi I, Vashaee D and Tayebi L 2012a Aqueous sol–gel synthesis of zirconium titanate (ZrTiO$_4$) nanoparticles using chloride precursors. *Ceram. Int.* 38(8): 6145-6149.

Salahinejad E, Hadianfard M, Macdonald D, Mozafari M, Vashaee D and Tayebi L 2012b Zirconium titanate thin film prepared by an aqueous particulate sol–gel spin coating process using carboxymethyl cellulose as dispersant. *Mater. Lett.* 88: 5-8.

Salahinejad E, Hadianfard M, Macdonald D, Mozafari M, Vashaee D and Tayebi L 2013 Multilayer zirconium titanate thin films prepared by a sol–gel deposition method. *Ceram. Int.* 39(2): 1271-1276.

Shao GN, Elineema G, Quang DV, Kim YN, Shim YH, Hilonga A, Kim JK and Kim HT 2012a Two step synthesis of a mesoporous titania–silica composite from titanium oxychloride and sodium silicate. *Powder Technol.* 217: 489-496.

Shao GN, Engole M, Imran SM, Jeon SJ, and Kim HT 2015a Sol–gel synthesis of photoactive kaolinite-titania: effect of the preparation method and their photocatalytic properties. *App. Surf. Sci.* 331: 98-107.

Shao GN, Hilonga A, Jeon SJ, Lee JE, Elineema G, Quang DV, Kim JK and Kim HT 2013a Influence of titania content on the mesostructure of titania–silica composites and their photocatalytic activity. *Powder Technol.* 233: 123-130.

Shao GN, Hilonga A, Kim YN, Kim JK, Elineema G, Quang DV, Jeon SJ and Kim HT 2012b Peptization technique in the synthesis of titania–silica composites and their photocatalytic properties. *Chem. Eng. J.* 198-199: 122-129.

Shao GN, Imran SM, Jeon SJ, Engole M, Abbas N, Haider SM, Kang SJ and Kim HT 2014 Sol–gel synthesis of photoactive zirconia–titania from metal salts and investigation of their photocatalytic properties in the photodegradation of methylene blue. *Powder Technol.* 258: 99-109.

Shao GN, Imran SM, Jeon SJ, Kang SJ, Haider SM and Kim HT 2015b Sol–gel synthesis of vanadium doped titania: Effect of the synthetic routes and investigation of their photocatalytic properties in the presence of natural sunlight. *Appl. Surf. Sci.* 351: 1213-1223.

Shao GN, Kim YN, Imran SM, Jeon SJ, Sarawade PB, Hilonga A, Kim JK and Kim HT 2013b Enhancement of porosity of

sodium silicate and titanium oxychloride based TiO_2–SiO_2 systems synthesized by sol–gel process and their photocatalytic activity. *Micropor. Mesopor. Mat*. 179: 111-121.

Sheikh R, Shao GN, Khan Z, Abbas N, Kim HT and Park YH 2015 Esterification of oleic acid by heteropolyacid/TiO_2-SiO_2 catalysts synthesized from less expensive precursors. *Asia-Pac. J. Chem. Eng.* 10(3): 339-346.

Simeone D, Baldinozzi G, Gosset D and Le CS 2006 Phase transition of pure zirconia under irradiation. *Nuc. Instrum. Methods Phys. Res. B* 250(1): 95-100.

Simeone D, Bechade JL, Gosset D, Chevarier A, Daniel P, Pilliaire H, and Baldinozzi G 2000 Investigation on the zirconia phase transition under irradiation. *J. Nuc. Mater.* 281(2): 171-181.

Spijksma GI, Huiskes C, Benes NE, Kruidhof H, Blank DHA, Kessler VG and Bouwmeester HJM 2006 Microporous zirconia–titania composite membranes derived from diethanolamine-modified precursors. *Adv. Mater.* 18(16): 2165-2168.

Srinivasan R, De Angelis RJ, Ice G and Davis BH 1991 Identification of tetragonal and cubic structures of zirconia using synchrotron x-radiation source. *J. Mater. Res.* 6(6): 1287-1292.

Stichert W and Schüth F 1998 Influence of crystallite size on the properties of zirconia. *Chem. Mater.* 10(7): 2020-2026.

Tanemura S, Miao L, Jin P, Kaneko K, Terai A and Nabatova-Gabain N 2003 Optical properties of polycrystalline and epitaxial anatase and rutile TiO_2 thin films by rf magnetron sputtering. *Appl. Surf. Sci*. 212–213: 654-660.

Verma A, Dwivedi R, Prasad R and Bartwal KS 2013 Microwave-assisted synthesis of mixed metal-oxide nanoparticles. *J. Nanopart.* 2013 (Article ID 737831).

Yan J, Li X, Cheng S, Ke Y, and Liang X 2009 Facile synthesis of titania-zirconia monodisperse microspheres and application for phosphopeptides enrichment. *Chem. Commun*. 20: 2929-2931.

Yuan Q, Liu Y, Li LL, Li ZX, Fang CJ, Duan WT, Li XG and Yan CH 2009 Highly ordered mesoporous titania–zirconia photocatalyst for applications in degradation of rhodamine-B and hydrogen evolution. *Micropor. Mesopor. Mater*. 124 (1–3): 169-178.

Zhao N, Pan D, Nie W and Ji X 2006 Two-phase synthesis of shape-controlled colloidal zirconia nanocrystals and their characterization. *J. Am. Chem. Soc*. 128 (31): 10118-10124.